Accepted Manuscript

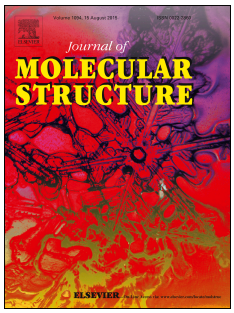

Ionic conductivity mediated by hydrogen bonding in liquid crystalline 4-*n*-alkoxybenzoic acids

Andrew Watmough Brown, Alfonso Martinez-Felipe

PII: S0022-2860(19)30916-0

DOI: https://doi.org/10.1016/j.molstruc.2019.07.072

Reference: MOLSTR 26825

To appear in: *Journal of Molecular Structure*

Received Date: 11 June 2019

Revised Date: 14 July 2019

Accepted Date: 16 July 2019

Please cite this article as: A.W. Brown, A. Martinez-Felipe, Ionic conductivity mediated by hydrogen bonding in liquid crystalline 4-*n*-alkoxybenzoic acids, *Journal of Molecular Structure* (2019), doi: https://doi.org/10.1016/j.molstruc.2019.07.072.

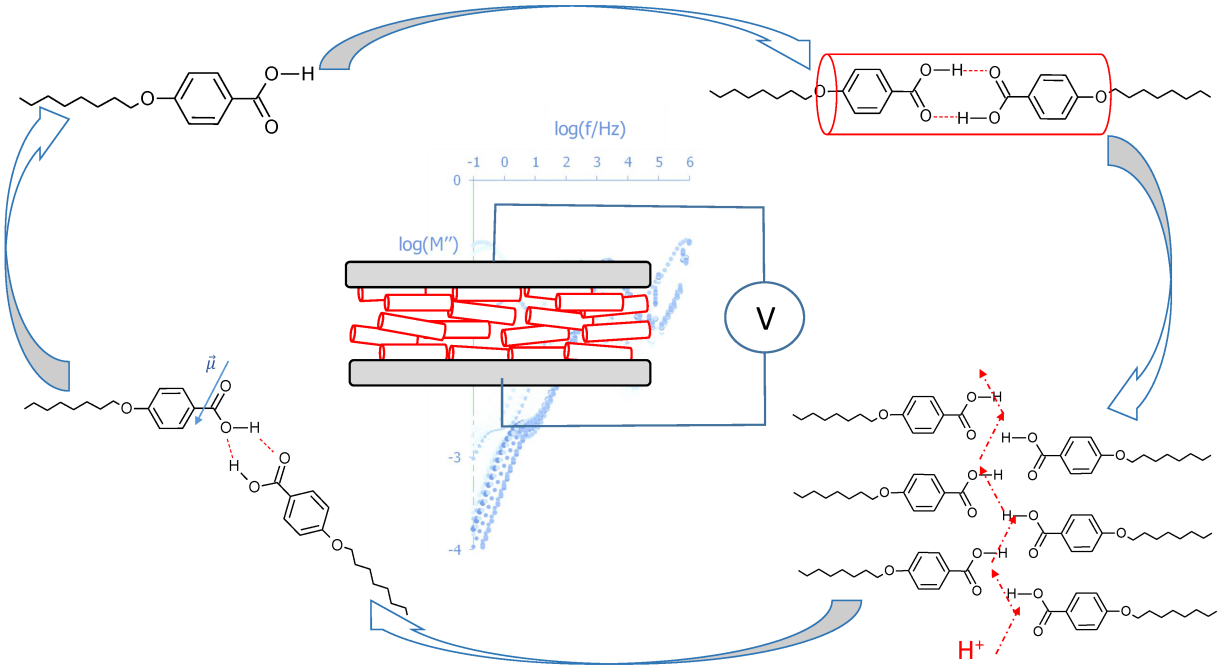

Manuscript

Title

Ionic conductivity mediated by hydrogen bonding in liquid crystalline 4-*n*-alkoxybenzoic acids.

Andrew Watmough Brown[1], Alfonso Martinez-Felipe[1,*]

[1.]Chemical and Materials Engineering Group, School of Engineering, University of Aberdeen. King's College, Aberdeen AB24 3UE, UK.

* Corresponding author, a.martinez-felipe@abdn.ac.uk

Abstract

We describe the dielectric response of a series of liquid crystalline 4-*n*-alkoxybenzoic acids, *n*OBAs, with different alkyl chains, *n* = 4, 5, 7 and 8, in planarly aligned cells, as potential anhydrous electrolytes for electrochemical cells. All *n*OBAs display two modes of dielectric relaxations and conductivity. At moderate-high frequencies, f ~ 10^1 to 10^4 Hz, the so-called *mode 1* involves fast dipole rearrangements leading to direct current, DC, conductivities in the σ_{dc1} ~ 10^{-5} S cm^{-1} range, which are eventually insensitive to bias fields. At lower frequencies, f ~ 10^{-1} to 10^1 Hz, the so-called *mode 2* is related to slower processes with lower DC conductivities, σ_{dc2} ~ 10^{-6} S cm^{-1}, which are further facilitated under sufficiently strong bias fields. Whilst *mode 1* can be associated to the presence (and motions) of asymmetric dimers stabilised by hydrogen bonding and free acids in the nematic phase, *mode 2* may involve the extension of the hydrogen-bonded network to longer ranges, probably by the formation of catemeric species, and its conductivity increases on heating in both the nematic and isotropic phases. Even though the conductivity values fall below those of benchmark electrolytes used in fuel cells (σ_{dc} ~ 0.1 S cm^{-1}), our results are promising, particularly for non-doped/non-hydrated electrolytes, and highlight the potential of the *n*OBAs and other hydrogen-bonded liquid crystals as components of electrolytes for ion conductivity.

Keywords

Liquid crystalline electrolytes; ion hopping; proton conductivity; 4-*n*-alkoxybenzoic acids; impedance spectroscopy; hydrogen-bonded liquid crystals.

1. Introduction

The development of electrolytes with high ionic conductivity under specific operation conditions is paramount to consolidate new electrochemical devices for energy conversion and storage applications [1]. Fuel cells, for example, convert chemical energy into electric work with high efficiencies and low emissions [2]. One unsolved challenge of low temperature fuel cells is to achieve high proton conductivity through the electrolyte, from anode to cathode, in the absence of solvents and dopants. Current benchmark electrolytes, like Nafion, need to be hydrated in the fuel cells to achieve high proton conductivity, through the so-called vehicular transport (H_3O^+). As a result, operation temperatures are capped to prevent water evaporation, and fuel cells undergo severe fuel crossover and efficiency losses when using polar liquid fuels, like methanol or ethanol [3]. Anhydrous electrolytes with high conductivities will allow to operate at higher temperatures without evaporation concerns, to use cheaper catalysts less sensitive to poisoning (*e.g.*, CO), and to reduce fuel crossover [4].

Liquid crystals hold promise as alternative electrolytes, in order to facilitate ion (proton) conductivity mechanisms in the absence of solvents [5]. Their local mobility can promote ion-hopping transport between neighbouring molecules, whilst their long-range order net ionic conductivity between anode and cathode [6-9]. Recently, we have developed a series of liquid crystalline polymers containing polar sulfonic groups as electrolytes in electrochemical devices [10-13]. Even though the conductivity values obtained in these and other liquid crystals are promising ($\sigma_{dc} \leq 10^{-4}$ S cm^{-1} range), a breakthrough is still necessary to compete with benchmark electrolytes, such as Nafion (σ_{dc}~0.1 S cm^{-1}) [3]. Moreover, the costly synthetic steps required to include the sulfonic groups as conducting units, can represent further technical constrains.

In this work, we evaluate the potential of a series of commercially available 4-*n*-alkoxybenzoic acids, the *n*OBAS, ***1***, as components of electrolytes in electrochemical cells,

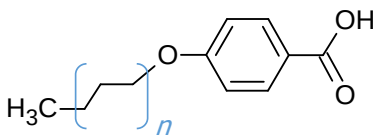

1, *n*OBAs

Our motivation is two-fold. First, to reduce viscosity by using low molar mass compounds, which will ultimately increase molecular (and ionic) mobility. Second, to promote hydrogen bonding between the acids as an intrinsic drive for proton conductivity, based on localised

ion hopping. To do this, we carry out an exhaustive dielectric study of four *n*OBAs analogues with different chain lengths, *n*, as a function of temperature, frequency and the presence of bias electric fields. Due to the role of dipole moments and molecular anisotropy on the interactions responsible for the formation of mesophases, dielectric analysis is particularly suitable to study the structural and electro-responsive properties of liquid crystals[14-22]. We believe that the molecular mechanisms investigated *via* the macroscopic electric properties of the *n*OBAs, will open new strategies to use non-expensive benzoic acids, as well as other hydrogen-bonded compounds, as components of fuel cells electrolytes.

2. Experimental procedure

Preparation and phase behaviour of the nOBAs

Four 4-*n*-alkoxybenzoic acids, *n*OBAs, ***1***, have been analysed, containing alkoxy chains with different lengths: *n*= 4, 5, 7 and 8 ($CH_3(CH_2)_{n-1}O$). The *n*OBAs are well-known mesomorphic materials, and are widely considered as the first examples of supramolecular liquid crystals with extended linearity, stabilised by hydrogen bonding, see **Figure 1** [23-28]. A recent review on the applications and thermal behaviour of *n*OBAs can be found, for example, in [29].

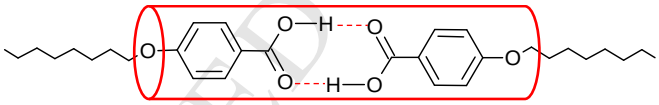

Figure 1. (nOBA)$_2$ symmetric dimer stabilised by hydrogen bonding (dotted lines) between benzoic acids, showing the linear supramolecular core.

All *n*OBAs in the present study were purchased from Sigma-Aldrich, except 4-pentoxybenzoic acid, 5OBA, which was supplied by TCI EUROPE N.V. All compounds were purified by recrystallisation from ethanol and hot filtration, followed by drying at 50℃, under vacuum overnight (Thermo Scientific Vacuum Oven). The purity of the *n*OBAs was confirmed to an accuracy of 99.5% *via* nuclear magnetic resonance spectroscopy, ^{1}H NMR, in $CDCl_3$, using a Bruker 300 MHz NMR spectrometer. Their phase transitions were assessed by differential scanning calorimetry, DSC, using a Mettler Toledo DSC821 module [29]. Thermograms were obtained by heat, cool and reheat cycles, with a heating rate of 10° min^{-1}, under nitrogen.

The liquid crystal behaviour of the *n*OBAs was identified by polarised optical microscopy, POM, using an Olympus BH-2 optical microscope equipped with a Linkam THMS 600

heating stage and a TMS 91 control unit. Nematic phases were characterised by Schlieren textures with two- and four-point singularities, which flashed when subjected to mechanical stress. Smectic C phases were also characterised by Schlieren textures, but with only one type of singularity and no homeotropic regions. All compounds exhibit nematic phases, and 7OBA and 8OBA also show additional smectic C phases in narrow ranges. The phase behaviour of the four *n*OBAs is summarised in **Table 1** [29], and is in excellent agreement with previous reports [30].

Dielectric characterisation and analysis

The dielectric and conductivity response of the *n*OBAs was studied by complex impedance spectroscopy. Indium Tin Oxide cells, ITO (SG100A080uG180, Instec), were filled by capillary with *n*OBAs in the melt state, to yield anti-parallel alignments with 1°to 3°pre-tilted angles, as confirmed by POM. Cells had $A = 100\, mm^2$ active areas, with 100 Ω resistance and $v = 8.0\, \mu m$ thickness. The capacitance of the cell, C_O, was then calculated as,

$$C_O = \epsilon_O \frac{A}{v} = 1.10675 * 10^{-10} F$$

where $\epsilon_O = 8.854 \cdot 10^{-12}\, F \cdot m^{-1}$, is the dielectric permittivity of vacuum.

The ITO cells were connected to a PARSTAT MC multichannel potentiostat (Ametek) and were placed on a Linkham TMS 91 hot stage for temperature control (±0.1 ^{o}C). The dielectric measurements consisted of isothermal frequency sweeps between 10^6 Hz and 0.1 Hz, with V_{rms}= 1000 mV amplitude alternating electric fields, and were taken first in the absence of bias electric fields (V_{bias} = 0 V). Then, the isothermal frequency sweeps were repeated under the application of different bias fields, V_{bias} =1 - 7 V. Experiments were carried out by cooling from the isotropic state (T=181^{o}C) to around 100^{o}C (at the crystal or smectic C ranges). Samples were labelled with the name of the 4-*n*-alkoxybenzoic acid (*n*OBA), followed by the temperature of the measurement in Celsius (for example, T120C), and the bias electric field applied (0 V to 7 V).

Several complex variables were calculated, as a function of the frequency, ω (rad·s^{-1}), the temperature, T, and the bias field, V_{bias}. The complex impedance, Z^*, was expressed as:

$$Z^*(\omega) = Z' + j\, Z''$$

where Z' and $Z''$are the real and imaginary impedance components, respectively, and j is the imaginary unit, $\sqrt{-1}$.

The complex permittivity, $\varepsilon^*(\omega) = \varepsilon' - j\varepsilon''$, was also calculated, according to:

$$\epsilon^* = \frac{1}{j\omega C_O Z^*}$$

with $\epsilon' = \frac{Z''}{\omega C_O |Z|}$, the elastic permittivity and , $\varepsilon'' = \frac{Z'}{\omega C_O |Z|}$, the dielectric loss factor.

The complex electric modulus, $M^*(\omega) = M' + jM''$, was also studied, in order to discriminate polarisation and conductive effects [31] :

$$M^* = \frac{1}{\varepsilon^*} = \frac{1}{\varepsilon' - \varepsilon''} = \frac{\varepsilon'}{\varepsilon'^2 + \varepsilon''^2} + j\frac{\varepsilon''}{\varepsilon'^2 + \varepsilon''^2}$$

with $M' = \frac{\varepsilon'}{\varepsilon'^2 + \varepsilon''^2}$ and $M'' = \frac{\varepsilon''}{\varepsilon'^2 + \varepsilon''^2}$.

The conductivity of the samples was quantified through the complex variable, $\sigma^*(\omega) = \sigma' + j\sigma''$, [32]

$$\sigma^* = \varepsilon^* \varepsilon_0 \omega$$

calculated as $\sigma' = \omega\epsilon_0\epsilon''$ and $\sigma'' = \omega\epsilon_0\epsilon'$.

Unless stated otherwise, the frequency, f, was expressed in hertz, with $f = \omega / 2\pi$.

3. Results and discussion

Conductivity and dielectric modes. Effect of bias electric fields

In **Figure 2**, 8OBA illustrates the dielectric response of the 4-*n*-alkoxybenzoic acids, *n*OBAs, in the nematic phase. The Nyquist plot of 8OBA-T130C-0V, obtained in the absence of direct current (DC) bias electric fields, V_{bias} = 0 V, depicts one semi-circle associated to a dielectric process with low impedance, appearing at high frequencies, log(f/Hz) > 1, which will be hereinafter denoted as *mode 1*, **Figure 2(a)**. At lower frequencies, another process appears, with higher impedance and capacitance, so-called *mode 2*. As expected, the application of bias fields modifies the dielectric response of 8OBA, and **Figure 2(b)** depicts

the case of 8OBA-T130C-7V as a representative example, V_{bias} = 7 V. The maximum in the Nyquist arc corresponding to *mode 2* is now visible, indicative of a decrease in impedance in its frequency range.

The corresponding complex permittivity and conductivity values were calculated, as described in the experimental section, and the results are plotted in **Figure 3** for 8OBA-T130C-7V. Both modes have associated DC processes, visible as plateaus in the log(σ'(f)) plots, and as maxima of the ε'' curves (shifted to lower frequencies [33]). The corresponding direct current conductivity values can be estimated from the σ' (f) plateaus, falling in the $\sigma_{dc,2}$ ~$10^{-6.1}$ S cm^{-1} range for *mode 2*, which is considerably high for non-doped liquid crystalline materials [6-8, 10].

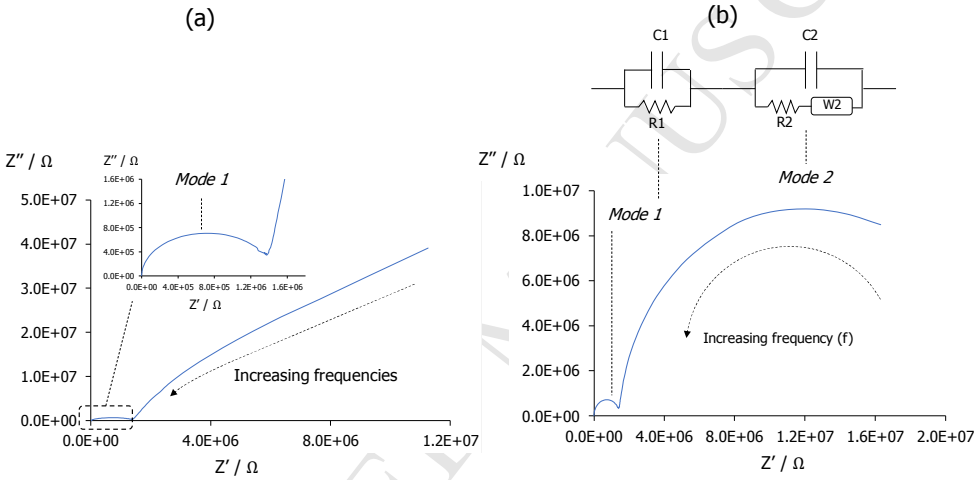

Figure 2. Nyquist plots corresponding to: (a) 8OBA-T130C-0V (b) and 8OBA-T130C-7V.

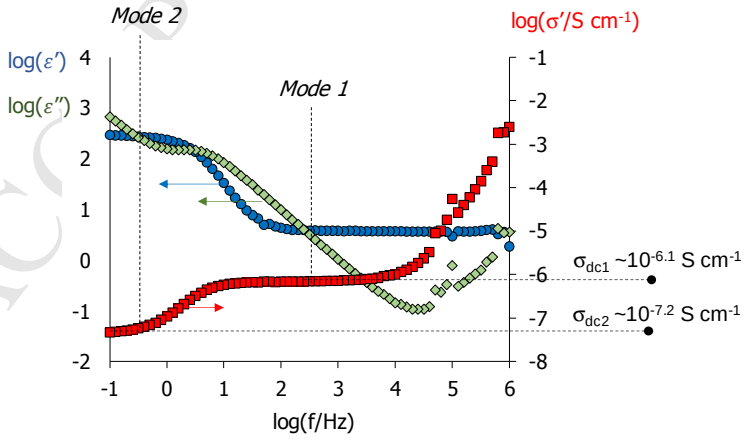

Figure 3. Double logarithmic plots of the elastic dielectric constant (●, ε'), dielectric loss (◆, ε'') and real component of the complex conductivity (■, σ'), as a function of the frequency, f, corresponding to 8OBA-T130C-7V.

The conductivity plateaus corresponding to the two modes coincide with maxima in the M'' curves [31], and overlap with Z'' peaks, see **Figure 4**. These results imply that both conductivity processes are associated to long-range ion diffusion, and not only to simple dipole rearrangements [34]. The Bode plots suggest that *mode 1* has a strong capacitive component, with the phase angle close to $\Theta \sim 90°$, **Figure ESI.1**, and the equivalent circuits were obtained for 8OBA-T130C, see also **Figure 2(b)** [35]. Whilst *mode 1* is described by a simple capacitor/resistance array in parallel, typical of a Debye response of dielectric materials, *mode 2* is explained by the presence of a Warburg element, typical of long-range ionic conductivity, W.

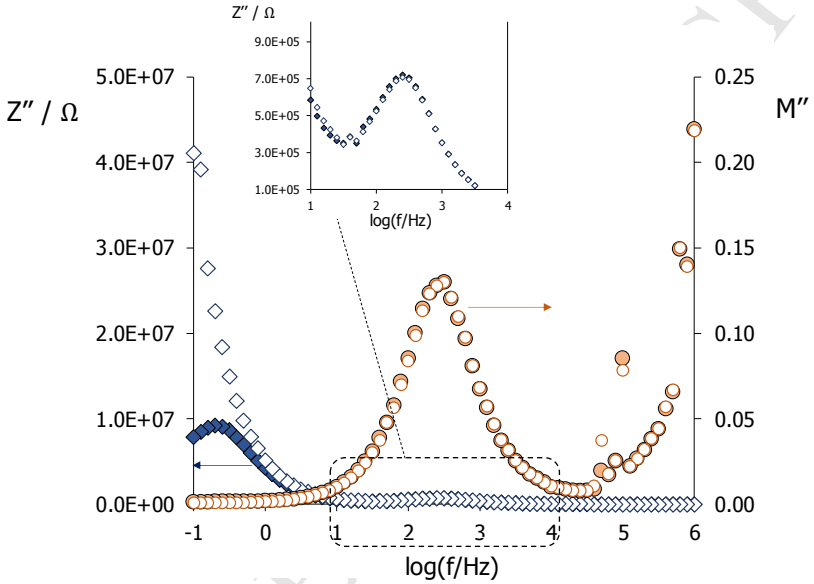

Figure 4. Comparison between the imaginary components of impedance, Z'' (◇, ◆) and electric modulus, M'' (○ , ●) for 8OBA-T130C-*X*V. Void symbols refer to results obtained in absence of electric fields, V_{bias} = 0 V (*X* = 0); filled symbols refer to results obtained under V_{bias} = 7 V (*X* = 7).

The effect of a progressive increase in bias voltages on 8OBA-T130C is shown in **Figure 5**, and the corresponding equivalent circuits were also calculated, see **Table 2**. Conductivity of *mode 2* increases in the presence of stronger DC fields, whilst *mode 1* remains largely unaffected. The capacitance values in **Table 2** for *mode 2* fall within the range of grain-boundary or interfacial polarisation effects (~10^{-9} F) [36], which may require collective rearrangements of dipoles and ions [37]. Hence, the sufficiently large relaxation times involved may be sensitive to the presence of DC fields. While $W2$ decreases asymptotically with V_{bias}, suggesting a limiting number of charges to be transported across 8OBA, the capacitance values, $C2$, increase linearly, **Figure ESI2**. Capacitance values of *mode 1*, $C1$,

on the other hand, are typical of bulk phenomena (~10^{-11} F), and can be associated to local dipole motions [37], hence less affected by DC electric fields. Conductivity related to this latter mode must be driven by short-range fluctuations related to proton hopping, occurring between the *n*OBAs molecules, and we will return to this observation later.

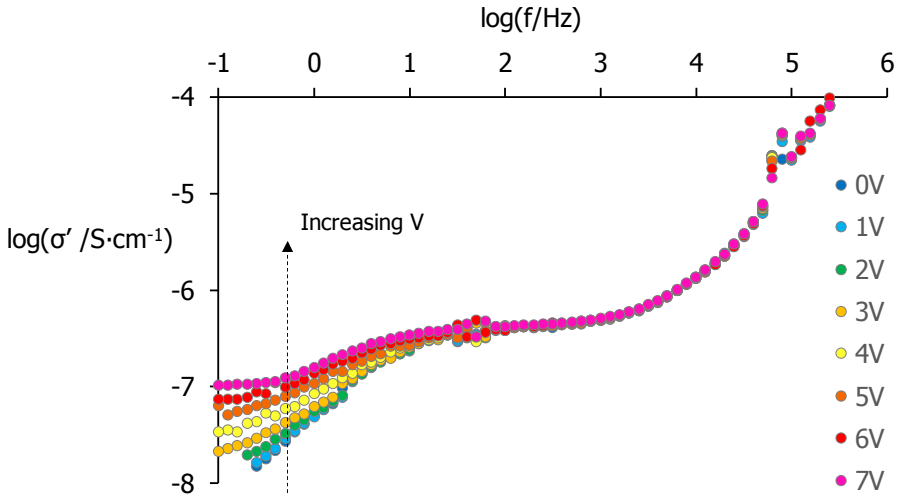

Figure 5. Effect of bias electric field (dotted arrow indicates increasing V_{bias}) on the real component of the complex conductivity for 8OBA-T130C-*X*V (*X* = 0 to 7).

Effect of temperature and phase behaviour

We now examine the effect of temperature on the dielectric and conductivity response of the 4-*n*-alkoxybenzoic acids, taking 8OBA as a model, in both the absence of bias electric fields (V_{bias} = 0 V), and under the maximum DC value (V_{bias} = 7 V). Comparable results are obtained for the rest of *nOBAs* and will be discussed with more detail in the next subsection. In **Figure 6** we show the log(σ'(f)) isothermal plots of 8OBA-TXC-0V, obtained at different temperatures on cooling from the isotropic melt, T=181°C, to the smectic C regime, T=100°C. At sufficiently high temperatures, the two modes discussed above are visible in the conductivity, **Figure 6(a)**, and electric modulus plots, **Figure 6(b)**. The highest conductivities are found in the isotropic phase, and then decrease on cooling, due to thermal activation of ion transport at higher temperatures, with step changes at the phase transitions, T_{NI}~145°C and T_{SmCN}~109°C, see **Table 1**. A similar temperature dependence is observed in the presence of electric fields, 8OBA-T*X*C-7V, even though the plateaus associated to DC conductivity in *mode* 2 are more evident through the whole temperature range, see **Figure 3** and also **Figure ESI3**.

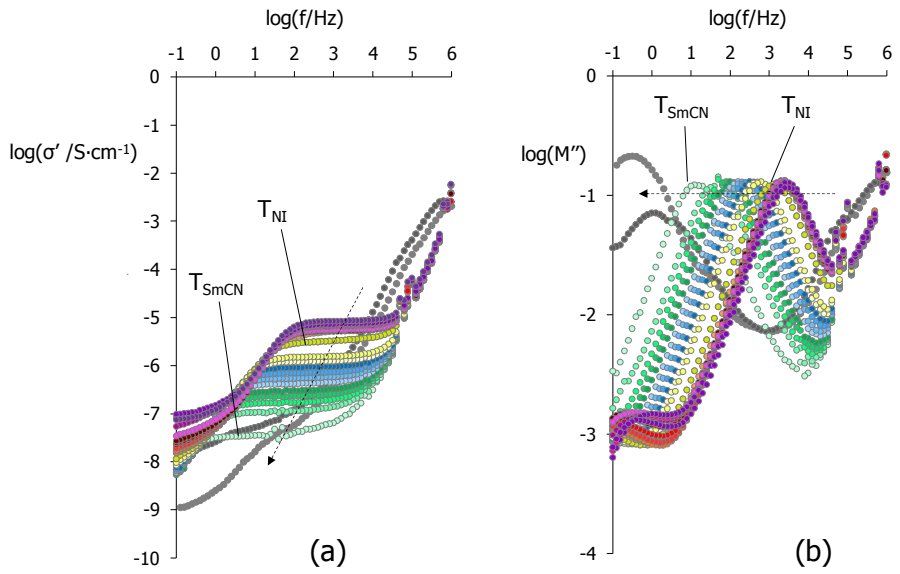

Figure 6. Temperature dependence of the dielectric response of 8OBA-T*X*C-0V in the frequency domain, corresponding to: (a) real conductivity, log(σ'(f)); (b) imaginary component of the electric modulus, log(M''(f)). T_{NI}, nematic to isotropic transition; T_{SmCN}, smectic C to nematic transition. Dotted arrows indicate direction on cooling from T=181°C to T=100°C.

In order to quantify the effects of both temperature and bias fields on the dielectric response of the *n*OBAs, Arrhenius plots were obtained from the σ_{dc} values and the maxima frequency of the M'' peaks, see **Figure 7** for 8OBA, and the activation energies, E_a, were calculated considering the corresponding linear regions:

$$\ln(\sigma_{dc}) = \ln(\sigma_0) - \frac{E_a(\sigma_{dc})}{R}\frac{1}{T} \quad ; \quad \ln\left(f_{M''_{max}}\right) = \ln(f_0) - \frac{E_a(M'')}{R}\frac{1}{T}$$

where σ_0 and f_0 are pre-exponential factors, *T* is the absolute temperature, and *R* = 8.31 J (mol K)$^{-1}$ the gas constant. The E_a results are summarised in **Table 3**. Fittings were carried out on the linear regions of each phase, and square residual values of $R^2 \geq 0.99$ were obtained.

In the nematic range, the Arrhenius plots corresponding to *mode 1* follow well-defined linear profiles, with considerably high activation energies, indicating that the dipole reorganisations may involve some degree of cooperativeness [38-40]. The reduction in σ_{dc1} on cooling, can be

associated to an increase in the nematic order parameter, and we will return to this observation later. Bias electric fields seem to have limited effect on the σ_{dc1} values and the thermal activation of conductivity, but reduce slightly the activation energy of M'', see **Figure 7(b)**. In the isotropic phase, variations with temperature are much less acute (hence lower activation energies in **Table 3**). The increase in σ_{dc2} under bias voltages, on the other hand, is consistent with the occurrence of long-range phenomena in *mode 2*, and takes place in all the temperature range. Contrarily to *mode 1*, σ_{dc2} increases through the isotropic phase, **Figure 7(a)**, and there is not a clear change in trend at T_{NI}. It is worth mentioning, however, that, after the application of V_{bias}, E_a increases in the nematic phase, but remains essentially unchanged in the isotropic melt, indicating that *mode 2* still presents some degree of phase sensitivity.

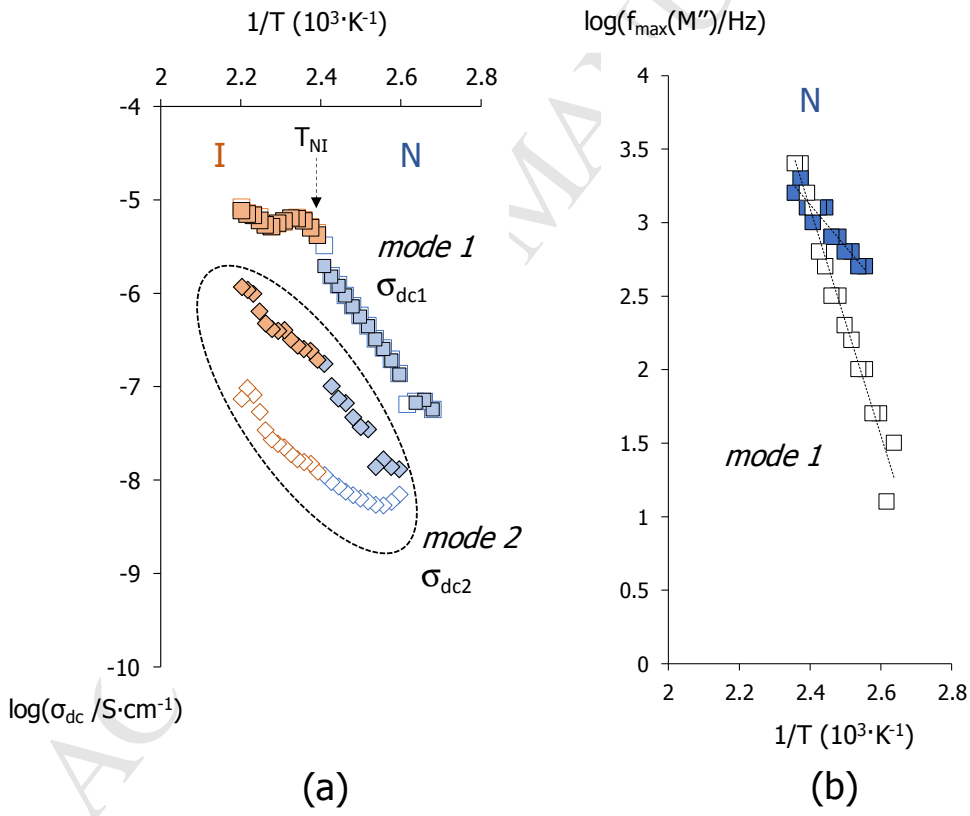

Figure 7. Arrhenius plots corresponding to 8OBA-T*X*C: (a) DC conductivity of *mode 1* (σ_{dc1}) and mode 2 (σ_{dc2}); (b) maxima of the electric modulus, M'', calculated for *mode 1*. Void symbols correspond to V_{bias} = 0 V, and filled symbols to V_{bias} = 7 V. I: isotropic phase; N: nematic phase.

Effect of the alkoxy chain length, n, on the dielectric conductivity response of nOBAs

We now compare the response of the four *n*OBAs under study in the nematic and isotropic phases, see **Figure 8**, and in **Figure 9** we show the Arrhenius plots for σ_{dc1} and σ_{dc2}, considering the effect of bias fields too. In general terms, the overall thermal activation of all samples agrees with the observations made above for 8OBA. Conductivity of *mode 1*, σ_{dc1}, is essentially insensitive to electric fields, **Figure 9(a)** and **9(c)**, whilst the application of V_{bias} increases the conductivity of *mode 2*, σ_{dc2}, **Figure 9(b)** and **9(d)**.

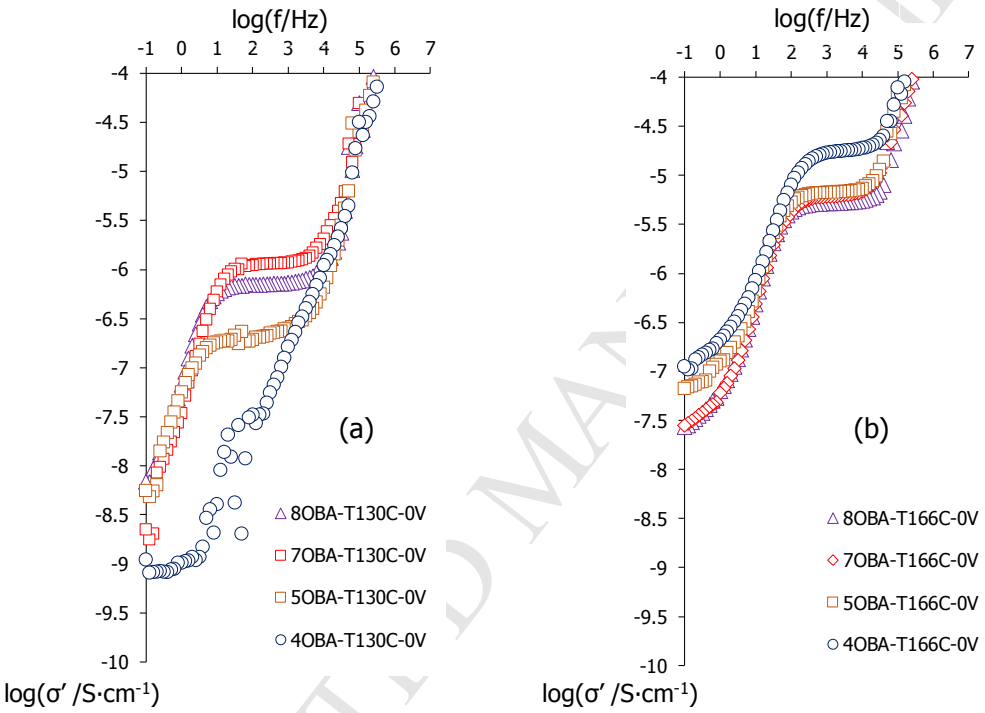

Figure 8. Compositional dependence of the conductivity, log(σ'(f)), for the *n*OBAs in the: (a) nematic range, T=130°C, nOBA-T130C-0V; and (b) isotropic range, T=166°C, nOBA-T166C-0V (V_{bias} = 0 V).

For *mode 1*, 8OBA and 7OBA display the highest conductivities in the nematic range, and 4OBA, in the isotropic range, see **Figures 8(a)** and **8(b)**, respectively. Whilst the σ_{dc1} values tend to plateau in the isotropic phases of these three samples, the dielectric response of 5OBA seems to be less phase sensitive, and shows a linear trend extending through the nematic and isotropic regimes, **Figures 9(a)** and **9(c)**. In the case of 4OBA, σ_{dc1} undergoes a sudden drop on cooling, at around T=150°C, due to its very narrow nematic range before crystallisation, see **Table 1**. These results confirm that conductivity, σ_{dc1}, is inversely dependent on the liquid crystal phase order. Interestingly, longer alkyl chains seem to

facilitate proton transfer in the nematic phase, *n* = 7, 8, whist the opposite occurs in the isotropic range.

All samples show comparable conductivity values for *mode 2*, σ_{dc2}, and electric fields have similar effects on all of them, with an average increase of around one order of magnitude by the application of V_{bias} = 7 V, **Figure 9(b)** and **9(d)**. For this mode, 4OBA also shows the highest σ_{dc2} values in the isotropic phase, with a drastic drop on cooling, attributed to crystallisation. As a general observation valid for both modes, the highest activation energies in the isotropic phases are found for the shorter chain analogues, 5OBA and 4OBA, whilst in the nematic phase, for the samples with longer chains, 7OBA and 8OBA.

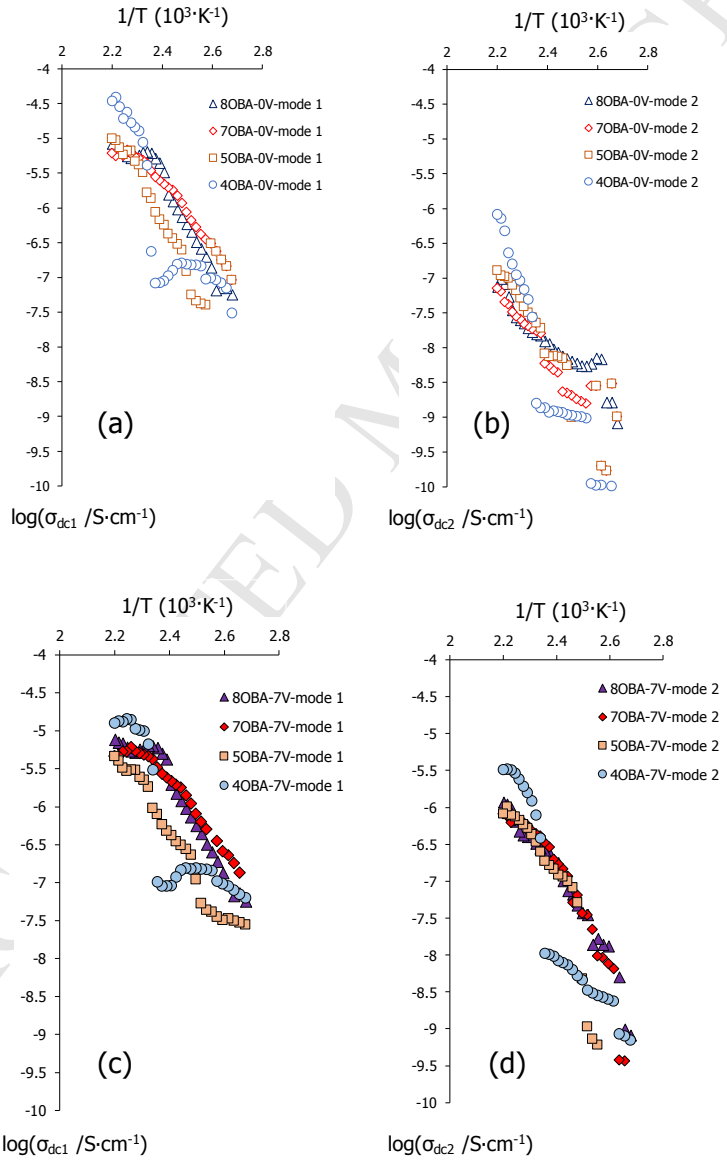

Figure 9. Arrhenius plots for the DC conductivity values, σ_{dc}, obtained for *mode 1*, (a) and (c); and *mode 2*, (b) and (d). Results obtained under V_{bias} = 0 V (a) and (b); and V_{bias} = 7 V (c) and (d).

From our previous observations, it is evident that *mode 1* is more sensible to chain length, *n*, and in **Figure 10** we have plotted the temperature dependence of the dielectric elastic constant, ε', obtained when fast molecular motions are prominent, *f* =1 Hz. Since samples are confined in planar cells, **Figure 10** must be mostly associated to the perpendicular component of the dielectric elastic constant, $\varepsilon_{\perp}$, and the drop in the nematic phase indicates that the *n*OBAs have positive anisotropy [41]. This is in agreement with the formation of symmetric dimers sketched in **Figure 1**, since the main molecular dipoles are associated to the O-H groups, which lay parallel to the main axis of the supramolecular dimer. As the order parameter of the nematic phase increases on cooling, this parallel alignment is favoured, resulting in the progressive reduction of $\varepsilon_{\perp}$ seen experimentally.

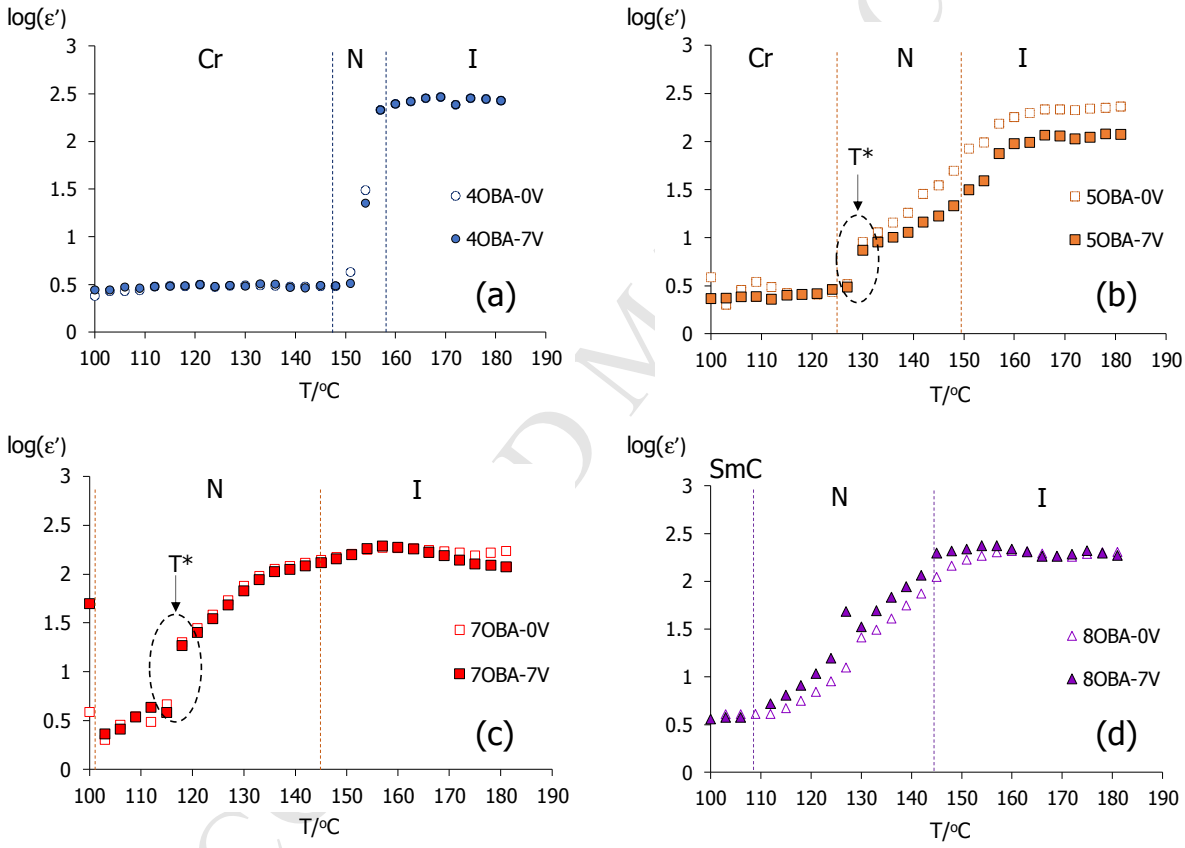

Figure 10. Dielectric elastic constant, ε', obtained at f = 1 Hz (*mode 1*), on cooling from the isotropic to the crystal and smectic C ranges: (a) 4OBA; (b) 5OBA; (c) 7OBA and (d) 8OBA. Results obtained under V_{bias} = 0 V (void symbols) and V_{bias} = 7 V (filled symbols). T* highlights step drops observed for 5OBA and 7OBA.

We know, however, that alkoxybenzoic acids can form several supramolecular species that coexist in temperature dependent equilibria[42], including: symmetric dimers, **Figure 1**, asymmetric dimers, free or "monomeric" acids and so-called catemers, **Figure 11** [43-45]. In planarly aligned samples, the dipole moments of some of these species will form certain angles with the ITO slides, and hence they may contribute to ε' in **Figure 10**. Indeed, *n*OBAs samples present considerably large amounts of asymmetric dimers at high temperatures [29, 42], and on cooling, these are progressively replaced by symmetric dimers, more compatible with the nematic field, causing the *mode 1* dielectric elastic constant (and conductivity) to decrease in **Figure 10**. Similar observations were reported previously by Kato [46, 47] and Petrov [48], who considered the presence of linear open dimers. The curved geometry of the asymmetric dimers in **Figure 11(b)**, which contain one free carbonyl group, C=O, may further contribute to the polarisability of electrolyte materials. The curved geometry of hydrogen-bonded asymmetric dimers favours, for example, intermolecular interactions that stabilise the twist-bend nematic phase, N_{TB} [49-55].

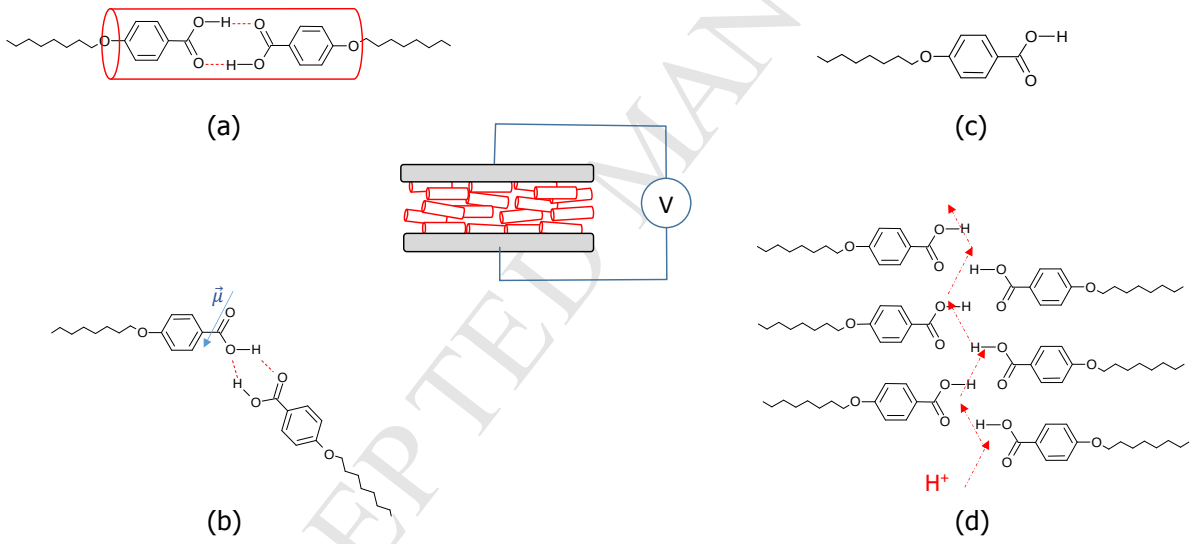

Figure 11. Supramolecular *n*OBA species stabilised by hydrogen bonding (dotted lines): (a) symmetric dimer; (b) asymmetric dimer, including the dipole moment associated to the non-hydrogen-bonded C=O group, $\vec{\mu}$; (c) free "monomeric" acids; (d) catemers. Dotted lines illustrate proton hopping assisted by hydrogen bonding.

Figure 10(b) and **(c)** also depict small step drops of ε' at the low temperature range of the nematic phases of 5OBA (T*~ 130°C) and 7OBA (T*~ 120°C), respectively, associated to the evolution of cybotatic nematic phases containing local "smectic-like" domains[56]. This pseudo-first order phase transition coincides with the removal of free acids after cooling

below certain temperature, $T^{\dagger}$, which recombine to form hydrogen-bonded species [29, 48]. Due to the high mobility of these monomeric species, **Figure 11(c)**, we believe that they may assist proton conductivity between other supramolecular species above $T^{\dagger}$ (T* in **Figure 10**) acting as dopants capable to establish dynamic hydrogen bonds, hence mediating ion hopping [57]. The recombination of *n*OBA monomers and dimers by hydrogen bonding on cooling, also promotes the formation of catemers, consisting of arrays of alkoxybenzoic molecules stabilised by lateral hydrogen bonding, see **Figure 11(d)** [29]. Similar long-range arrangements were previously associated to ion conductivity between contiguous acrylic alkoxybenzoic acids in nematic planar electrolytes [6]. Even though polymerisation (and further crosslinking) limited those conductivity values to the σ_{dc}~10^{-8} S·cm^{-1} range [58], they were comparable to our results obtained for *mode 2*, σ_{dc2}, and are consistent with the formation of longer-range ionic conductive pathways in *n*OBAs.

4. Concluding remarks

The 4-*n*-alkoxybenzoic acids undergo two modes of dielectric relaxation and conductivity. At low frequencies, the so-called *mode 2* exhibits values of DC conductivity in the σ_{dc2} ~ 10^{-10} S·cm^{-1} to $10^{-5.5}$ S·cm^{-1} range, associated to long-range diffusion of protons through the electrolytes, which are further promoted by the presence of bias fields. It is not possible to explain the improvement in conductivity of *mode 2* by a net perpendicular (homeotropic) realignment of the samples' director under these DC electric fields, since the highest field applied, V_{bias} = 7 V, falls below to the Fréederiscksz transition of the *n*OBAs (observed around V_{bias} = 15 V by polarised optical microscopy). Alternatively, it is possible that the electric fields mitigate defects between conducting domains (considering that the capacitance values fall within the so-called "grain-boundary" regimes) [59], ultimately facilitating long-range proton conductivity.

Mode 1, on the other hand, takes place at higher frequencies, and is based on local rearrangements of the dipoles in the *n*OBAs, associated to their hydrogen bonds. This mode provides higher conductivity values than *mode 2* and is more sensitive to phase behaviour. The conductivity in the nematic phase decreases on cooling due to an increase of the local order/parameter in the nematic field. Conductivity (σ_{dc1}) is linked to the existence and exchange between different hydrogen-bonded species. More precisely, we believe that asymmetric dimers (with a net dipole non-parallel to the electrodes in planarly aligned samples, see **Figure 11(b)**) and monomeric species (with high molecular mobility, **Figure**

11(c)) may act as proton bridges between symmetric dimers and catemers, this latter being more relevant to yield long-range conductivity.

To sum up, our results highlight the potential of the 4-*n*-alkoxybenzoic acids, *n*OBAs (and therefore similar benzoic acids), as ionic conductors, in the absence of dopants. More specifically, the results exhibited by 7OBA and 8OBA in the nematic range unveil an interesting strategy to control their anisotropic conductivity, and their activation energies, the potential to regulate conductivity with temperature. Introducing mechanisms to tune the equilibria between hydrogen-bonded *n*OBAs species, or including these materials into devices by supramolecular complexation, open exciting possibilities to achieve proton electrolytes under anhydrous conditions in electrochemical devices.

Acknowledgements

The authors would like to acknowledge Mathew Abdy and Daniel Zaton for their help preparing the samples, Prof. Corrie Imrie and Prof. John Storey for their continuous advice, and the School of Engineering (University of Aberdeen) for financial support.

References

1. Pereira EC, Cuesta A. A personal perspective on the role of electrochemical science and technology in solving the challenges faced by modern societies. J Electroanal Chem 2016 NOV 1;780:355-9.

2. Sharaf OZ, Orhan MF. An overview of fuel cell technology: Fundamentals and applications. Renewable & Sustainable Energy Reviews 2014 APR;32:810-53.

3. Mauritz KA, Moore RB. State of understanding of nafion. Chemical Reviews 2004 Oct;104(10):4535-85.

4. Schuster M, Meyer W. Anhydrous proton-conducting polymers. Annual Review of Materials Research 2003;33:233-61.

5. Martinez-Felipe A. Liquid crystal polymers and ionomers for membrane applications. Liquid Crystals 2011 2011;38(11-12):1607-26.

6. Liang T, van Kuringen HPC, Mulder DJ, Tan S, Wu Y, Borneman Z, Nijmeijer K, Schenning APHJ. Anisotropic dye adsorption and anhydrous proton conductivity in smectic liquid crystal networks: The role of cross-link density, order, and orientation. Acs Applied Materials & Interfaces 2017 OCT 11;9(40):35218-25.

7. Yang X, Tan S, Liang T, Wei B, Wu Y. A unidomain membrane prepared from liquid-crystalline poly(pyridinium 4-styrene sulfonate) for anhydrous proton conduction. J Membr Sci 2017 FEB 1;523:355-60.

8. Kobayashi T, Ichikawa T, Kato T, Ohno H. Development of glassy bicontinuous cubic liquid crystals for solid proton-conductive materials. Adv Mater 2017 JAN 25;29(4):1604429.

9. Yang J, Wang Y, Yang G, Zhan S. New anhydrous proton exchange membranes based on fluoropolymers blend imidazolium poly (aromatic ether ketonejs for high temperature polymer electrolyte fuel cells. Int J Hydrogen Energy 2018 APR 26;43(17):8464-73.

10. Vanti L, Mohd Alauddin S, Zaton D, Aripin NFK, Giacinti-Baschetti M, Imrie CT, Ribes-Greus A, Martinez-Felipe A. Ionically conducting and photoresponsive liquid crystalline terpolymers: Towards multifunctional polymer electrolytes. European Polymer Journal 2018 December 2018;109:124-32.

11. Martinez-Felipe A, Badia JD, Santonja-Blasco L, Imrie CT, Ribes-Greus A. A kinetic study of the formation of smectic phases in novel liquid crystal ionogens. European Polymer Journal 2013 JUN 2013;49(6):1553-63.

12. Martinez-Felipe A, Imrie CT, Ribes-Greus A. Study of structure formation in side-chain liquid crystal copolymers by variable temperature fourier transform infrared spectroscopy. Industrial & Engineering Chemistry Research 2013 Jul 3;52(26):8714-21.

13. Martinez-Felipe A, Lu Z, Henderson PA, Picken SJ, Norder B, Imrie CT, Ribes-Greus A. Synthesis and characterisation of side chain liquid crystal copolymers containing sulfonic acid groups. Polymer 2012 Jun 7;53(13):2604-12.

14. Salamon P, Eber N, Buka A, Gleeson JT, Sprunt S, Jakli A. Dielectric properties of mixtures of a bent-core and a calamitic liquid crystal. Physical Review E 2010 MAR;81(3):031711.

15. Elmahdy MM, Dou X, Mondeshki M, Floudas G, Butt H, Spiess HW, Muellen K. Self-assembly, molecular dynamics, and kinetics of structure formation in dipole-functionalized discotic liquid crystals. J Am Chem Soc 2008 APR 16;130(15):5311-9.

16. Panarin Y, Kalinovskaya O, Vij J. The investigation of the relaxation processes in antiferroelectric liquid crystals by broad band dielectric and electro-optic spectroscopy. Liquid Crystals 1998 AUG;25(2):241-52.

17. Sinha G, Aliev F. Dielectric spectroscopy of liquid crystals in smectic, nematic, and isotropic phases confined in random porous media. Physical Review E 1998 AUG;58(2):2001-10.

18. Urban S, Wurflinger A. Dielectric properties of liquid crystals under high pressure. Advances in Chemical Physics, Vol 98 1997;98:143-216.

19. Bouteiller L, LeBarny P. Polymer-dispersed liquid crystals: Preparation, operation and application. Liquid Crystals 1996 AUG;21(2):157-74.

20. VALLERIEN S, KREMER F, KAPITZA H, ZENTEL R, FRANK W. Field-dependent soft and goldstone mode in a ferroelectric liquid-crystal as studied by dielectric-spectroscopy. Physics Letters A 1989 JUN 26;138(4-5):219-22.

21. VALLERIEN S, KREMER F, BOEFFEL C. Broad-band dielectric-spectroscopy on side group liquid-crystal polymers. Liquid Crystals 1989 JAN;4(1):79-86.

22. Martinez-Felipe A, Santonja-Blasco L, Badia JD, Imrie CT, Ribes-Greus A. Characterization of functionalized side-chain liquid crystal methacrylates containing nonmesogenic units by dielectric spectroscopy. Ind Eng Chem Res 2013 JUL 3 2013;52(26):8722-31.

23. Bradfield AE, Jones B. Two apparent cases of liquid crystal formation. Journal of the Chemical Society 1929 1929:2660-1.

24. Gray GW, Jones B. Mesomorphism of some alkoxynaphthoic acids. Nature 1951 1951;167(4237):83-4.

25. Gray GW, Jones B. Influence of substituents on the mesomorphism of para-normal-alkoxybenzoic and 6-normal-alkoxy-2-naphthoic acids. Nature 1952 1952;170(4324):451-2.

26. Gray GW, Jones B. The mesomorphic transition points of the para-normal-alkoxybenzoic acids - A correction. Journal of the Chemical Society 1953 1953(DEC):4179-80.

27. Gray GW, Jones B. Mesomorphism and chemical constitution .3. the effect of halogen substitution on the mesomorphism of the 4-alkoxybenzoic acids. Journal of the Chemical Society 1954 1954(JUL):2556-62.

28. Gray GW, Jones B. Mesomorphism and chemical constitution .1. the normal-alkoxynaphthoic acids. Journal of the Chemical Society 1954 1954(FEB):683-6.

29. Abdy MJ, Murdoch A, Martinez-Felipe A. New insights into the role of hydrogen bonding on the liquid crystal behaviour of 4-alkoxybenzoic acids: A detailed IR spectroscopy study. Liquid Crystals 2016 OCT-DEC;43(13-15):2191-207.

30. Fonseca JMS, Santos LMNBF, Monte MJS. Thermodynamic study of 4-n-alkyloxybenzoic acids. J Chem Eng Data 2010 JUN 2010;55(6):2238-45.

31. HODGE I, INGRAM M, WEST A. New method for analyzing ac behavior of polycrystalline solid electrolytes. J Electroanal Chem 1975;58(2):429-32.

32. Dyre JC. Some remarks on ac conduction in disordered solids. J Non Cryst Solids 1991 11;135(2–3):219-26.

33. Wubbenhorst M, van Turnhout J. Analysis of complex dielectric spectra. I. one-dimensional derivative techniques and three-dimensional modelling. J Non Cryst Solids 2002 JUL 1;305(1-3):40-9.

34. Chan CH, Kammer H. Impedance spectra of polymer electrolytes. Ionics 2017 SEP;23(9):2327-37.

35. Yuan X, Song C, Wang H, Zhang J. Electrochemical impedance spectroscopy in PEM fuel cells: Fundamentals and applications. ; 2010. PT: B; UT: WOS:000272789000007.

36. Coster H, Chilcott T, Coster A. Impedance spectroscopy of interfaces, membranes and ultrastructures. Bioelectrochem Bioenerget 1996 AUG;40(2):79-98.

37. Guo L, Gomola K, Gorecka E, Pociecha D, Dhara S, Araoka F, Ishikawa K, Takezoe H. Transition between two orthogonal polar phases in symmetric bent-core liquid crystals. Soft Matter 2011;7(6):2895-9.

38. STARKWEATHER H. Noncooperative relaxations. Macromolecules 1988 JUN;21(6):1798-802.

39. Wojnarowska Z, Knapik J, Diaz M, Ortiz A, Ortiz I, Paluch M. Conductivity mechanism in polymerized imidazolium-based protic ionic liquid [HSO3-BVIm][OTf]: Dielectric relaxation studies. Macromolecules 2014 JUN 24;47(12):4056-65.

40. Delhorbe V, Bresser D, Mendil-Jakani H, Rannou P, Bernard L, Gutel T, Lyonnard S, Picard L. Unveiling the ion conduction mechanism in imidazolium-based poly(ionic liquids): A comprehensive investigation of the structure-to-transport interplay. Macromolecules 2017 JUN 13;50(11):4309-21.

41. Stocchero M, Ferrarini A, Moro G, Dunmur D, Luckhurst G. Molecular theory of dielectric relaxation in nematic dimers. J Chem Phys 2004 OCT 22;121(16):8079-97.

42. Martinez-Felipe A, Imrie CT. The role of hydrogen bonding in the phase behaviour of supramolecular liquid crystal dimers. J Mol Struct 2015 11/15;1100:429-37.

43. Xu H, Kang N, Xie P, Zhang RB. A new insight into the hydrogen-bonded liquid crystals built from carboxylic acids and pyridyl moieties. Molecular Crystals and Liquid Crystals 2002 2002;373:119-26.

44. Martinez-Felipe A, Cook AG, Abberley JP, Walker R, Storey JMD, Imrie CT. An FT-IR spectroscopic study of the role of hydrogen bonding in the formation of liquid crystallinity for mixtures containing bipyridines and 4-pentyloxybenzoic acid. Rsc Advances 2016;6:108164-79.

45. Martinez-Felipe A, Cook AG, Wallage MJ, Imrie CT. Hydrogen bonding and liquid crystallinity of low molar mass and polymeric mesogens containing benzoic acids: A variable temperature fourier transform infrared spectroscopic study. Phase Transitions 2014 DEC 2 2014;87(12):1191-210.

46. Kato T, Frechet JMJ, Wilson PG, Saito T, Uryu T, Fujishima A, Jin C, Kaneuchi F. Hydrogen-bonded liquid-crystals - novel mesogens incorporating nonmesogenic bipyridyl compounds through complexation between h-bond donor and acceptor moieties. Chemistry of Materials 1993 Aug;5(8):1094-100.

47. Kato T, Uryu T, Kaneuchi F, Jin C, Frechet JMJ. Hydrogen-bonded liquid-crystals built from hydrogen-bonding donors and acceptors - infrared study on the stability of the hydrogen-bond between carboxylic-acid and pyridyl moieties. Liquid Crystals 1993 May;14(5):1311-7.

48. Petrov M, Anachkova E, Kirov N, Ratajczak H, Baran J. Ir spectroscopic investigations of peculiar behavior of 4,n-alkoxybenzoic acids in their mesomorphic state .1. nonaligned samples. Journal of Molecular Liquids 1994 JUL 1994;61(1-3):221-30.

49. Meyer R. R. Balian, G. Weil, editors. Molecular fluids. New York: Gordon and Breach; 1976. .

50. Dozov I. On the spontaneous symmetry breaking in the mesophases of achiral banana-shaped molecules. Europhys Lett 2001 OCT 2001;56(2):247-53.

51. Cestari M, Diez-Berart S, Dunmur DA, Ferrarini A, de la Fuente MR, Jackson DJB, Lopez DO, Luckhurst GR, Perez-Jubindo MA, Richardson RM, et al. Phase behavior and properties of the liquid-crystal dimer 1 ",7 "-bis(4-cyanobiphenyl-4 '- yl) heptane: A twist-bend nematic liquid crystal. Physical Review E 2011 Sep 16;84(3).

52. Cestari M, Frezza E, Ferrarini A, Luckhurst GR. Crucial role of molecular curvature for the bend elastic and flexoelectric properties of liquid crystals: Mesogenic dimers as a case study. Journal of Materials Chemistry 2011 2011;21(33):12303-8.

53. Walker R, Pociecha D, Abberley JP, Martinez-Felipe A, Paterson DA, Forsyth E, Lawrence GB, Henderson PA, Storey JMD, Gorecka E, et al. Spontaneous chirality through mixing achiral components: A twist-bend nematic phase driven by hydrogen-bonding between unlike components. Chemical Communications 2018 APR 7;54(27):3383-6.

54. Paterson DA, Martinez-Felipe A, Jansze SM, Marcelis ATM, Storey JMD, Imrie CT. New insights into the liquid crystal behaviour of hydrogen-bonded mixtures provided by temperature-dependent FTIR spectroscopy. Liquid Crystals 2015;5-6:928-39.

55. Jansze SM, Martinez-Felipe A, Storey JMD, Marcelis ATM, Imrie CT. A twist-bend nematic phase driven by hydrogen bonding. Angewandte Chemie-International Edition 2015 JAN 7 2015;54(2):643-6.

56. Ilyin SO, Konstantinov II. Rheological evidence for the existence of subphases in the liquid crystalline 4-n-alkoxybenzoic acids. Liquid Crystals 2016 FEB 19 2016;43(3):369-80.

57. Liang T, Wu Y, Tan S, Yang X, Wei B. Enhancing proton conduction via doping of supramolecular liquid crystals (4-alkoxybenzoic acids) with imidazole. Chemical Physics Letters 2015 SEP 16;637:22-5.

58. Concellon A, Liang T, Schenning APHJ, Luis Serrano J, Romero P, Marcos M. Proton-conductive materials formed by coumarin photocrosslinked ionic liquid crystal dendrimers. Journal of Materials Chemistry C 2018 FEB 7;6(5):1000-7.

59. Kim M, Serra F. Tunable large-scale regular array of topological defects in nematic liquid crystals. Rsc Advances 2018;8(62):35640-5.

Tables

Ion conductivity mediated by hydrogen bonding in liquid crystalline 4-*n*-alkoxybenzoic acids.

Andrew Watmough Brown[1], Alfonso Martinez-Felipe[1,*]

[1,]Chemical and Materials Engineering Group, School of Engineering, University of Aberdeen. King's College, Aberdeen AB24 3UE, UK.

* Corresponding author, a.martinez-felipe@abdn.ac.uk

Table 1. Transition temperatures corresponding to the *n*OBAs, obtained by differential scanning calorimetry, DSC, in cooling scans.

***n*OBA**	T_{CrN}[a] T_{CrSmC}[b]	T_{SmCN}*	T_{NI}**
4OBA	146.8[a]	-	158.9
5OBA	124.4[a]	-	150.1
7OBA	92.7[b]	99.0	144.9
8OBA	101.7[b]	108.5	144.6

Temperatures (/ ^{o}C) corresponding to: [a]Crystal to Nematic transition; [b]Crystal to Smectic C transition; *Smectic C to Nematic transition; **Nematic to Isotropic transition.

Table 2. Elements of the equivalent circuits corresponding to 8OBA-T130C-XV, obtained under different *bias* electric fields, *X* = 0 V to 7 V (Ri, resistance, Ci capacitance, Wi Warburg element) for *modes i = 1* ($R1$, $C1$) and *i=2* ($R2, C2, W2$).

Bias voltage / Volt	$R1$ / Ω ·10^{-4}	$C1$ / F ·10^{11}	$R2$/ Ω ·10^{-7}	$C2$/ F·10^{9}	$W2$ / Ω·s^{-1}
0 (no bias)	9.71	7.6	1.04	8.9	10.8
1	9.72	7.6	1.13	9.5	9.3
2	9.87	7.8	1.30	12.0	6.4
3	9.70	7.7	1.31	16.5	4.6
4	9.79	7.8	0.93	26.5	4.0
5	9.69	7.7	1.06	32.8	2.9
6	9.80	7.8	0.92	42.4	2.6
7	9.96	8.0	0.79	55.1	2.3

Table 3. Activation energies, E_a (kJ·mol^{-1}) obtained from *modes 1* and *2* of the different *n*OBA, corresponding to the DC conductivity values (σ_{dc}) and frequency of M'' peak maxima f_{max} (M''). I: isotropic phase; N, nematic phase.

	σ_{dc1} ***mode 2***		σ_{dc2} ***mode 1***		f_{max} **(M'')** ***mode 1***	
Sample	**I**	**N**	**I**	**N**	**I**	**N**
8OBA-0V	55.9	47.7	16.5	115.5	16.5	132.8
8OBA-7V	55.3	100.3	15.2	115.1		141.1
7OBA-0V	47.9	81.2	51.6	102.9	28.4	106.7
7OBA-7V	77.2	128.8	45.4	107.5	19.2	85.9
5OBA-0V	111.8	29.6	67.7	97.8	76.4	104.3
5OBA-7V	66.6	98.1	66.0	63.8	37.5	69.2
4OBA-0V	210.4	-	86.1	59.6	52.7	
4OBA-7V	79.8	44.6	24.7		22.5	

"Ionic conductivity mediated by hydrogen bonding in liquid crystalline 4-*n*-alkoxybenzoic acids"

Highlights

4-*n*-alkoxybenzoic acids, *n*OBAs, are readily available ionic conducting electrolytes.

Linear anisotropy of hydrogen bonded dimers promotes aligned superstructures for ion conductivity.

High anisotropic conductivity in nematic ranges is based on local molecular and dipole motions.

Long-range conductivity is associated to catemeric arrays and lateral hydrogen bonding.

Equilibria between different hydrogen bonded species can control the conductivity of benzoic acid electrolytes.

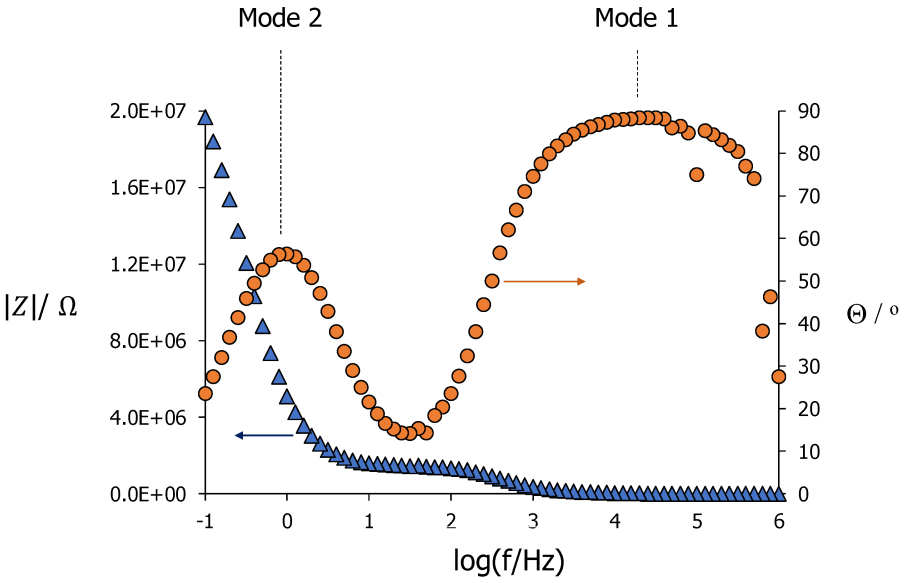

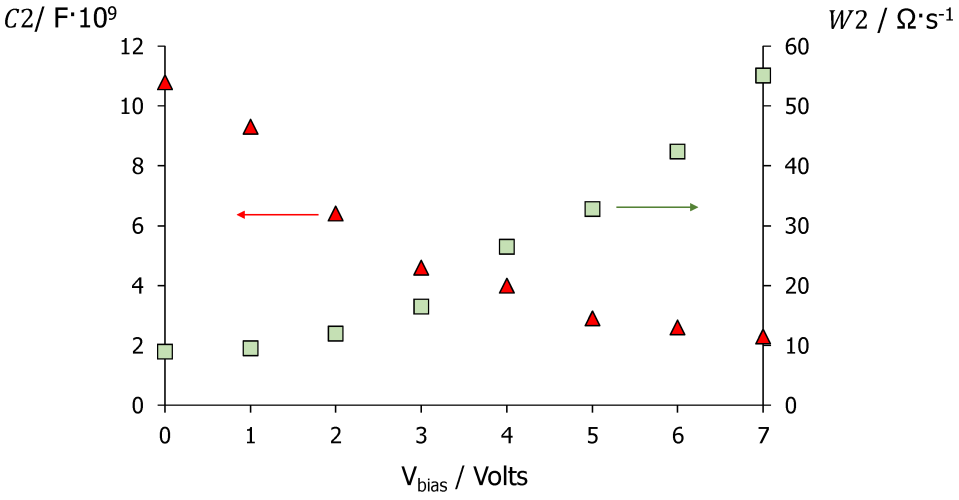

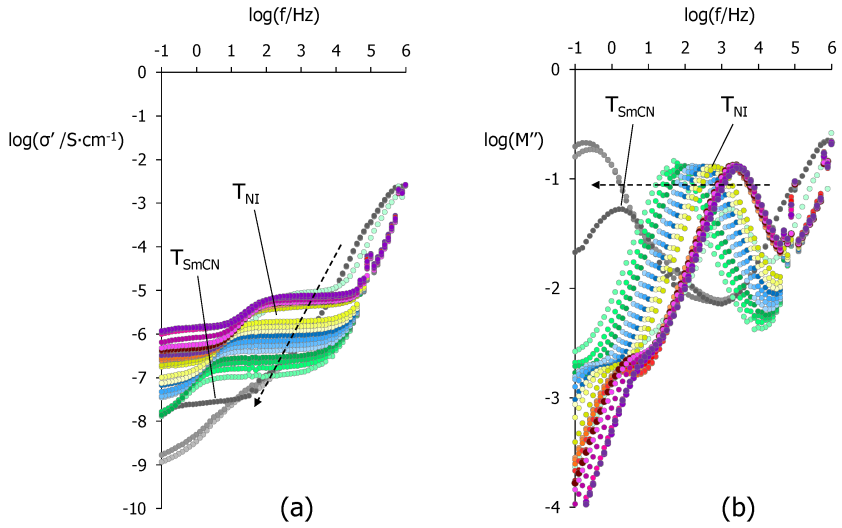

Electronic Supplementary Information

Ionic conductivity mediated by hydrogen bonding in liquid crystalline 4-*n*-alkoxybenzoic acids.

Andrew Watmough Brown[1], Alfonso Martinez-Felipe[1,*]

[1.]Chemical and Materials Engineering Group, School of Engineering, University of Aberdeen. King's College, Aberdeen AB24 3UE, UK.

* Corresponding author, a.martinez-felipe@abdn.ac.uk

Contents

- Figures ESI1 to ESI3.

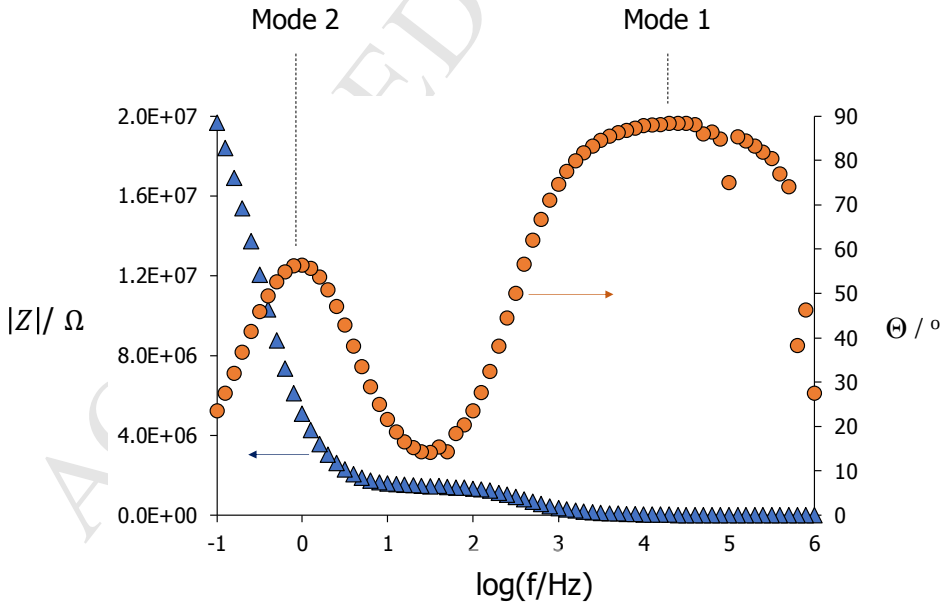

Figure ESI1. Bode plots corresponding to the impedance modulus, $|Z|$ (▲), and phase, Θ (●), corresponding to 8OBA-T130C-*X*V.

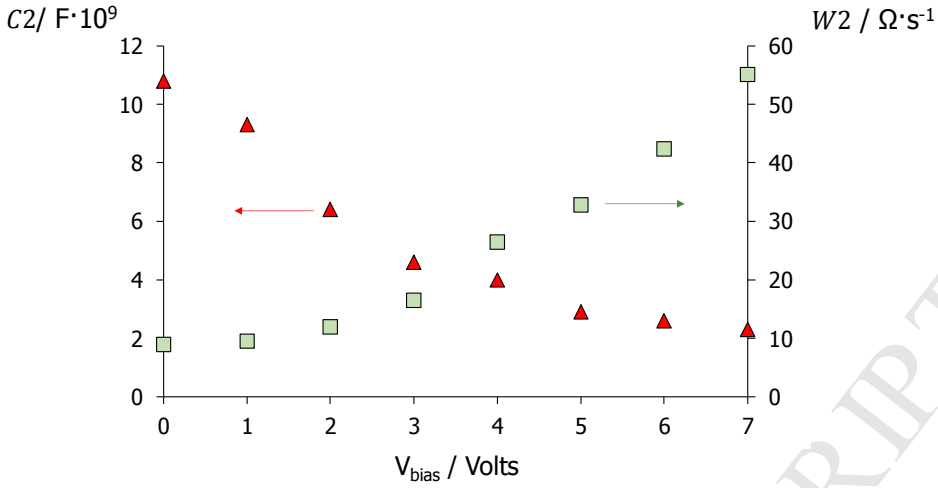

Figure ESI2. Effect of bias electric field, *X*, on the capacitance, $C2$ (▲), and Warburg element, $W2$ (■), in the equivalent circuits corresponding to 8OBA-T130C-*X*V.

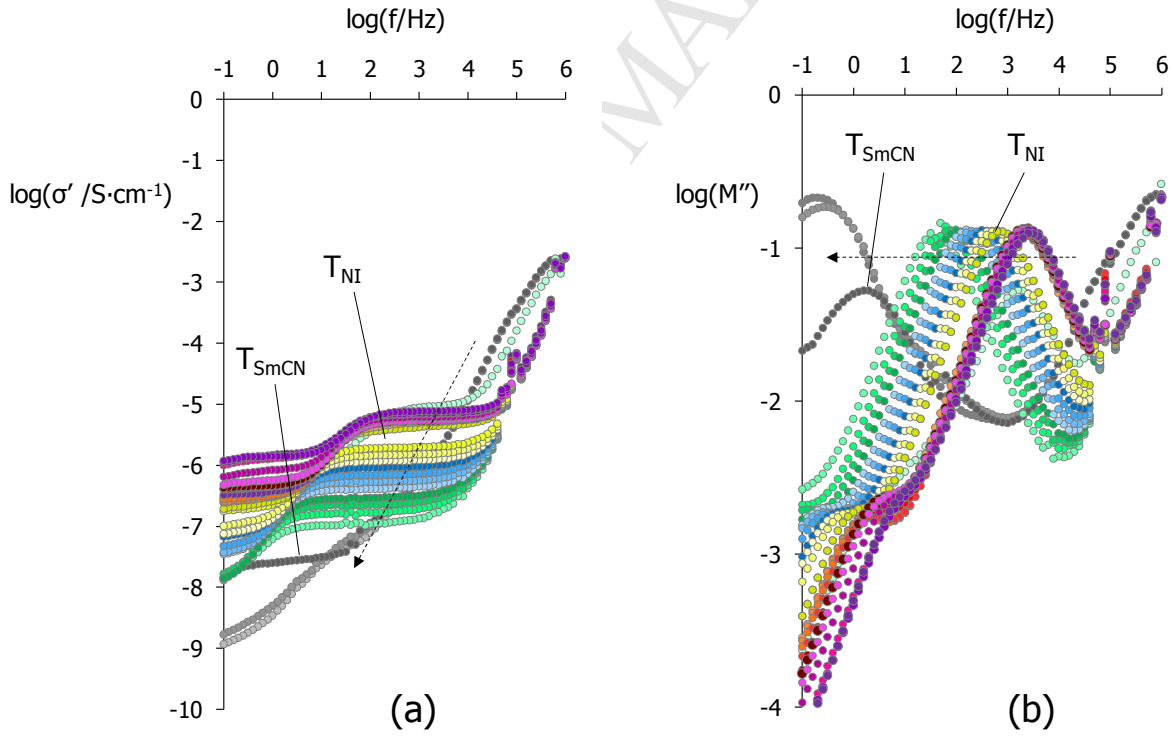

Figure ESI3. Temperature dependence of the dielectric response of 8OBA-T*X*C-7V in the frequency domain, corresponding to: (a) real conductivity, log(σ'(f)); (b) imaginary component of electric modulus, log(M''(f)). T_{NI}, nematic to isotropic transition; T_{SmCN}, smectic C to nematic transition. Dotted arrows indicate direction on cooling from T=181°C to T=100°C.